J Fluoresc (2007) 17:727–738
DOI 10.1007/s10895-007-0181-5

ORIGINAL PAPER

Single-molecule Detection of Reactive Oxygen Species: Application to Photocatalytic Reactions

Takashi Tachikawa · Tetsuro Majima

Received: 20 January 2007 / Accepted: 12 March 2007 / Published online: 24 April 2007

Abstract In this review, we have focused on the oxidation reactions of single dye molecules by reactive oxygen species (ROS). The methodologies for the single-molecule detection of ROS, such as hydroxyl radical ($HO^{\bullet}$), singlet oxygen ($O_2(a^1\Delta_g)$), and hydrogen peroxide (H_2O_2), have been introduced together with examples. In particular, a successful application using the single-molecule fluorescence technique for the investigation of the TiO_2 photocatalytic oxidation reactions is demonstrated in detail.

Keywords Single-molecule fluorescence spectroscopy · Reactive oxygen species · TiO_2 photocatalyst · Photooxidation

Introduction

Reactive oxygen species (ROS), according to their own name, have higher reactivity than molecular oxygen in the ground state $\left({}^3O_2\left(X^3\Sigma_g^-\right)\right)$ [1, 2]. The ROS designation comprehends not only free radicals, such as superoxide radical ($O_2^{\bullet -}$), hydroperoxyl radical ($HO_2^{\bullet}$), hydroxyl radical ($HO^{\bullet}$), peroxyl radical ($ROO^{\bullet}$), and alkoxyl radical ($RO^{\bullet}$), but also non-radicals, namely hydrogen peroxide (H_2O_2), singlet oxygen ($^1O_2(a^1\Delta_g)$), and hypochlorous acid (HOCl).

T. Tachikawa · T. Majima (✉)
The Institute of Scientific and Industrial Research (SANKEN),
Osaka University, Mihogaoka 8-1, Ibaraki,
Osaka 567-0047, Japan
e-mail: majima@sanken.osaka-u.ac.jp

The $^1O_2(a^1\Delta_g)$ molecule is one of important ROS in atmospheric, biological, and therapeutic processes and is also used as a reagent in organic synthesis [3–14]. The energy diagram of O_2 molecules and the reported peak wavelengths of absorption, fluorescence, and phosphorescence spectra are summarized in Scheme 1.

Today, it is well-known that $^1O_2(a^1\Delta_g)$ molecule is a highly energetic oxygen molecule, which can oxidize organic molecules, resulting in the photodegradation. In the early 1930s, Kautsky suggested the possibility that $^1O_2(a^1\Delta_g)$ molecules might be involved as the reactive intermediate during dye-sensitized photooxygenation reactions [7–10]. He demonstrated that excitation of sensitizer molecules adsorbed on silica gel caused the oxygenation of acceptor molecules absorbed on a different set of silica gel particles, which are physically separated from the dye-coated ones. From this experimental result, it was concluded that the oxygenation must have involved formation of some metastable species which was capable of migrating in the gas phase from the sensitizer to the acceptor, and suggested that this species was $^1O_2(a^1\Delta_g)$ molecules. Although Kautsky's proposal was not generally accepted during his lifetime, it was eventually supported by later works by the groups of Khan and Kasha [11, 12], Foote and Wexler [13], and Corey and Taylor [14]. To date, variants of the Kautsky experiment have been performed, and the development of both applications and novel observation techniques has strongly accelerated in the past decade [4].

Recently, it has been reported that $^1O_2(a^1\Delta_g)$ molecules are directly or indirectly generated via energy or electron

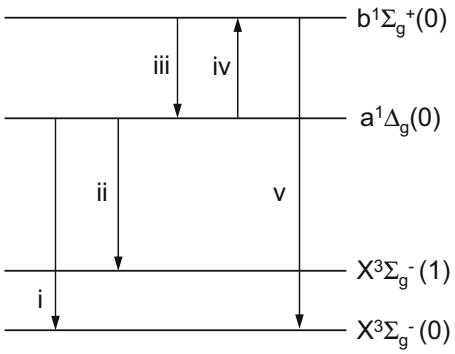

i) $a^1\Delta_g(0) \rightarrow X^3\Sigma_g^-(0)$: 1270 nm phosphorescence
ii) $a^1\Delta_g(0) \rightarrow X^3\Sigma_g^-(1)$: 1590 nm phosphorescence
iii) $b^1\Sigma_g^+(0) \rightarrow a^1\Delta_g(0)$: 1925 nm fluorescence
iv) $a^1\Delta_g(0) \rightarrow b^1\Sigma_g^+(0)$: 1925 nm absorption
v) $b^1\Sigma_g^+(0) \rightarrow X^3\Sigma_g^-(0)$: 762 nm phosphorescence

Scheme 1 Energy levels of molecular oxygen

transfer reactions between $^3O_2\left(X^3\Sigma_g^-\right)$ and semiconductor nanomaterials, such as silicon [15], titanium dioxide (TiO_2) [16–18], and CdSe quantum dots [19]. Although the generation yields of $^1O_2(a^1\Delta_g)$ molecules from these materials in solution are much lower than those from organic dye sensitizers [20], the materials will be the basis of newly emerging nanobiotechnologies because of their temporal stability [21–23].

The TiO_2 photocatalysts have been extensively studied and used for the water-splitting reaction that produces hydrogen, the degradation of organic pollutants, the surface wettability conversion, and so on [21, 24–29]. It has been reported that various ROS, such as $O_2^{\bullet-}$ [30, 31], $^1O_2(a^1\Delta_g)$ [16–18], $HO^{\bullet}$ [32], and H_2O_2 [33], are generated on the TiO_2 surface in the gas and liquid phases. The proposed photocatalytic reaction schemes for the generation of ROS were summarized in Scheme 2.

Recently, Tatsuma et al. reported the remote photocatalytic oxidation of organic and inorganic materials using the TiO_2 photocatalyst [34–37]. They explained this phenomenon in terms of a double excitation scheme in which the photodecomposition of gaseous H_2O_2 by UV light to give $HO^{\bullet}$ is the key process.

The scientific research in the field of ROS associated with biological and non-biological functions is continuously requiring new sensitive and specific tools that may enable a deeper insight on its action mechanisms. However, ROS present some characteristics that make them difficult to be detected, namely their very short lifetime and high reactivity, and the variety of antioxidants existing in vivo, capable of capturing these species. It is, therefore, essential to develop methodologies capable of overcoming this type of obstacles. The fluorescence methodology, associated with the use of suitable probes, is an excellent approach to measure ROS because of its high sensitivity, simplicity in data collection, and high spatial resolution in microscopic imaging techniques [38].

In particular, the metastable and reactive ROS, such as $^1O_2(a^1\Delta_g)$ and $HO^{\bullet}$, have a finite lifetime in any system in which it is produced. The magnitude of this lifetime can vary over a large range and is governed by the constituents of the medium in which ROS exist. Thus, much would be gained if tenuous ROS in air, solution, polymer, and biological systems could be directly monitored with both time and spatial resolutions. For two decades, Ogilby and co-workers have developed several spectroscopic techniques to quantify the diffusion coefficients of O_2 molecules in solution, polymer films, and biological cell [39–42]. In their approach, the O_2 sorption into the polymer is monitored using the near-infrared phosphorescence (around 1,270 nm, see Scheme 1) of $^1O_2(a^1\Delta_g)$ produced via photosensitizaion. They successfully detected the phosphorescence of $^1O_2(a^1\Delta_g)$ using fluorescence microscopy equipped with a cooled near-IR photomultiplier tube operated in a photon counting mode. More recently, it has been demonstrated that $^1O_2(a^1\Delta_g)$ can also be monitored in the region of 5,100–5,300 cm^{-1} (around 1925 nm, see Scheme 1), which is assigned to the $O_2\left(a^1\Delta_g\right) - {}^1O_2\left(b^1\Sigma_g^-\right)$ (see Scheme 3) transition, from air-saturated polystyrene samples using a microscope attached to a step-scan Fourier transform IR spectrometer [42]. One advantage of this approach is that both kinetic and spectroscopic data are obtained in a single experiment. Of course, this technique also has its limitations, the most significant of which reflects the fact that weak transitions are generally difficult to monitor in an absorption experiment. However, as they mentioned, this approach complements the $^1O_2(a^1\Delta_g)$ emission experiments and thus, in some cases, allows us to examine systems that might otherwise be inaccessible.

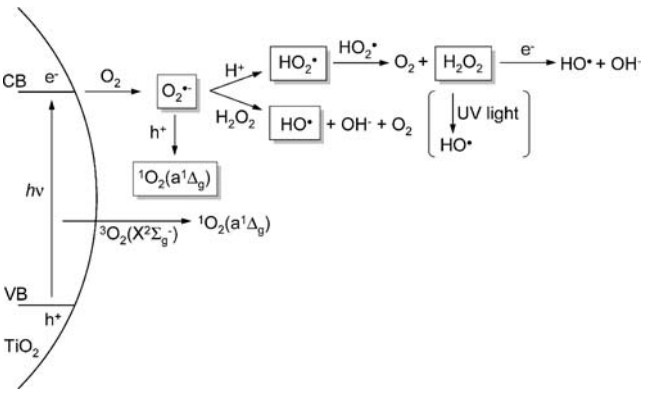

Scheme 2 Generation of ROS during TiO_2 photocatalytic reactions

Scheme 3 Single-molecule detection of the airborne $O_2(a^1\Delta_g)$ with TDI

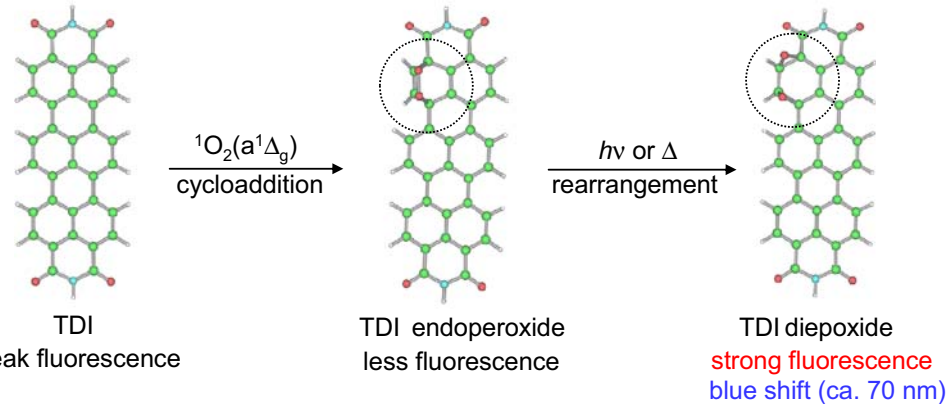

The main goal of this short review is to present the fluorescence methodologies that have been used for detecting ROS, especially, $^1O_2(a^1\Delta_g)$, at the single-molecule level. As is well-known, single-molecule fluorescence studies can reveal the detailed kinetics of physical processes and chemical reactions that are often hidden in ensemble measurements [43–45]. First, we discuss the photooxidation processes of dye molecules by $^1O_2(a^1\Delta_g)$ studied by the single-molecule spectroscopy. The single-molecule measurements have yielded many insights into photophysical and photochemical processes of single dye molecules in various environments. Next, we introduce our recent works for the detection of airborne ROS. The authors and coworkers have successfully applied the single-molecule technique to clarify the bleaching processes of single dye molecules during the remote TiO_2 photocatalytic oxidation reactions. Moreover, an airborne $^1O_2(a^1\Delta_g)$ molecule diffused from the surface of the TiO_2 nanoparticles was detected at the single-molecule level. We also introduce research works for the detection of H_2O_2 at the single-molecule level. Finally, we suggest future directions for the applications of the single-molecule spectroscopy toward the heterogeneous reaction systems, such as photocatalytic reactions.

Photooxidation processes of single dye molecules

The current understanding, though far from being complete, suggests an important role of $^1O_2(a^1\Delta_g)$ that is created in the immediate vicinity of the molecule by self sensitization involving triplet–triplet annihilation [46–57]. In most single-molecule experiments in ambient air, the photobleaching can be attributed to photooxidation reactions with $^1O_2(a^1\Delta_g)$, although this is only the case at low dye concentrations ($<10^{-5}$ M) in the ensemble experiments. Thus, the diffusion constant and solubility of oxygen in the host matrix are important factors in the efficiency of photooxidation reactions. In the case of poly(vinyl alcohol) (PVA), for example, the diffusion of O_2 molecules is enhanced when water is present in the polymer, softening its structure [49].

The single-molecule spectral jump or shift and lifetime changes correlated with intensity fluctuations processes let us know the changes in the nanoenvironment and photoinduced reactions. In 2001, Basché et al have proposed that some of the photooxidation products of single terrylene molecules in a *p*-terphenyl host crystal are peroxides and diepoxides [46]. As shown in Fig. 1a, various types of

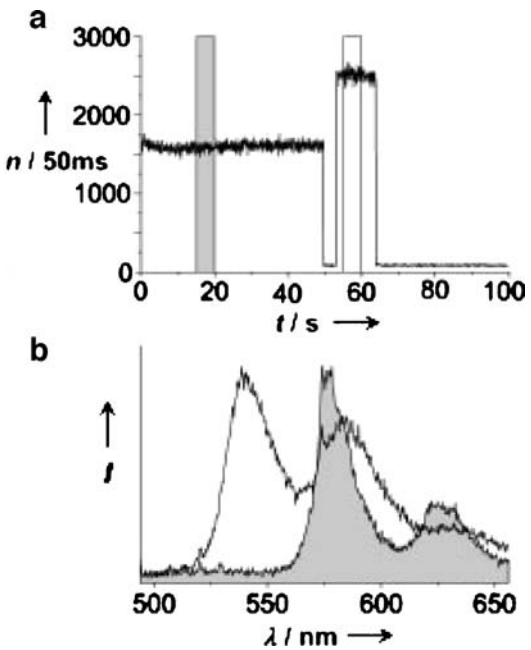

Fig. 1 Fluorescence intensity of a single terrylene molecule in *p*-terphenyl as a function of time (emission time trace) in air. After a dark-state transition the molecules resumes emission at a different intensity level (**a**). Fluorescence spectra taken during the time periods (**b**). After the dark-state transition the spectrum is shifted by 40 nm to the blue. Copyright WILEY-VCH Verlag GmbH, D-69451 Weinheim, 2001

intensity changes are observed under ambient conditions. Interestingly, the fluorescence signal jumps to a new level after having dropped to the background level for a short period of time. In addition to the time traces, a complete sequence of single-molecule emission spectra is recorded simultaneously at regular intervals of 5 s. The spectra shown in Fig. 1b, which belong to the time traces indicated by filled bars with corresponding colors, suggests that after the terrylene molecule resumes emission at around 53 s the spectrum has shifted to the shorter wavelength by 40 nm. They attribute all the intensity and spectral changes to a photooxidation of terrylene or subsequent internal rearrangements of the primary photoproducts. A similar spectral shift was found for a multichromophoric rigid polyphenylenic dendrimer with spectrally different rylene chromophores using single-molecule spectroscopy [47].

One of the most intriguing and most intensely studied features of single-molecule fluorescence is fluorescence intermittency which is often referred to as a photoblinking. This behavior refers to the temporal disappearance of emitted light when molecules undergo reversible transitions between "on" and "off" states, whereas photobleaching is an irreversible process where bleached products that do not absorb or emit at the excitation and emission wavelengths, respectively, are formed from the molecule.

Photoblinking behavior has been observed for a wide range of emitters and cannot be explained by intersystem crossing alone. Especially, in contrast to the well-understood triplet mechanism, the nature of slow blinking of single molecules on a millisecond to second time scale is not yet unambiguously recognized. According to the literature, the power law distributions indicate the existence of a wide distribution of dark state lifetimes rather than well-defined lifetimes as expected for the triplet state [54].

To date, several models are discussed as being responsible for the occurrence of these long-lived dark states: (a) modification of the chromophore's conformation shifting the absorption away from the excitation or reducing the fluorescence quantum yield (b) reversible photochemical processes like formation of an ionized or a metastable oxidized state; (c) quenching by nearby molecules. The time scales of fluorescence intermittency attributed to the various processes are similar, requiring additional information in order to identify the underlying mechanism.

Recently, Barbara et al. studied the bias dependence of the fluorescence "flickering" of a single isolated poly [2-methoxy,5-(2′-ethylhexyloxy)-*p*-phenylene-vinylene] (MEH-PPV) molecule in a poly(methyl methacrylate) (PMMA) polymer matrix and obtained information on the oxidation and reduction properties of the intermediate [55]. Figure 2 shows the fluorescence modulation of a single MEH-PPV molecule by photooxidation and an electrical bias. As the single-MEH-PPV molecule became photooxidized

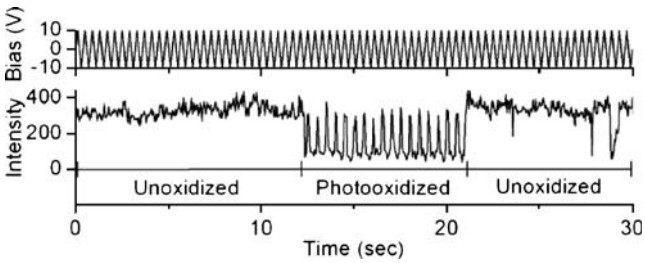

Fig. 2 Fluorescence modulation of a single MEH-PPV molecule by photooxidation and an electrical bias. A triangle voltage sequence was repeatedly applied to the device (*upper trace*) while collecting fluorescence transients (*lower trace*). Copyright 2004 American Chemical Society

at t=12 s, the electric bias-induced modulation of the fluorescence significantly increased in magnitude. Correspondingly, when the molecule reverted spontaneously to its unoxidized form at t=21 s, the bias-dependent modulation was diminished. This approach allows for the first direct correlation of photobleaching and charge carrier effects for the same nanometer-scale region of a conjugated polymer.

Interestingly, the deoxygenation has been found to decrease [50, 52], even increase [53], or to leave the photobleaching quantum yield mainly unaffected [48, 56]. Removal of oxygen has been proposed as a remedy against photobleaching by photooxidation. On the other hand, interaction of O_2 with dyes in their metastable states, such as the triplet state, can lead to both ground state recovery and generation of irreversible photoproducts.

Renn et al. investigated the photobleaching of organic fluorophores embedded in PMMA polymer matrix using wide-field fluorescence microscopy [57]. They characterized the photostability of various type of dye molecules by measuring the 'bleaching number,' defined as the average number of photons a molecule emits until photobleaching occurs, and analysed the dependence of the bleaching number on the presence of O_2 molecules.

Figure 3 shows fluorescence time traces visualizing the influence of O_2 for Cy3 dye. Initially the sample was purged with N_2 gas, and the N_2 flow was then stopped allowing O_2 gas to penetrate the sample. The fluorescence of the sample is clearly stronger in the presence of O_2. It should be noted that an improvement of photostability in the presence of O_2 for other ionic dyes (DiI, TMR, Rh6G, and Alexa 546), suggesting that O_2 molecules quench the photoactive triplet state of dyes, but it only indirectly contributes to photochemistry. Considering that the primary influence of O_2 is usually the quenching of the triplet state, these findings indicate that the triplet state population of ionic dyes plays a significant role in photobleaching processes. They also found that a pronounced contribution of blinking at longer timescales for all dyes, and that this blinking is considerably reduced upon O_2 exposure. In

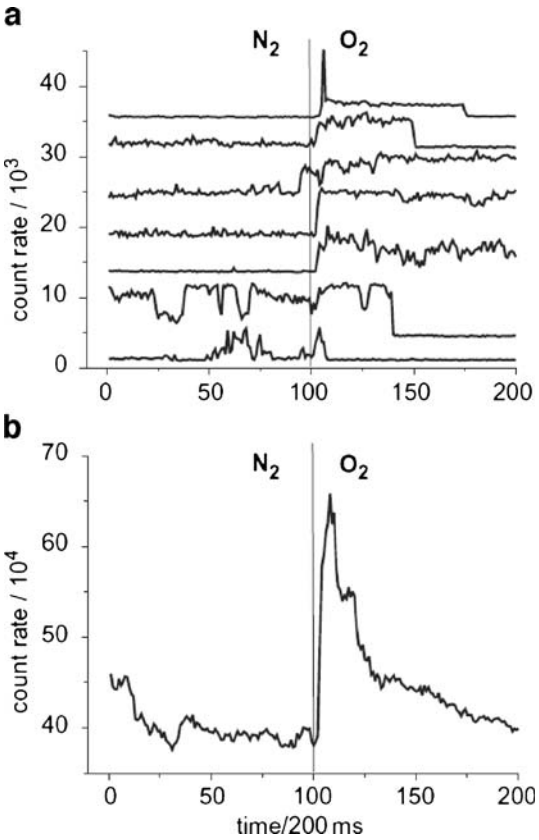

Fig. 3 **a** Single-molecule time traces visualizing the influence of O_2 for Cy3. Initially the sample was purged with N_2 gas. After 100 images the nitrogen flow was stopped allowing O_2 to penetrate the sample. The individual traces are shifted for better visibility. On average the fluorescence intensity increases when O_2 penetrates the sample. This is also shown in (**b**) where quasi bulk data, the sum of 65 single molecule time traces, is shown. Copyright 2006 Taylor & Francis

contrast, it was observed that photobleaching of the aromatic hydrocarbon terrylene is strongly enhanced by O_2.

Single-molecule detection of photocatalytically generated $^1O_2(a^1\Delta_g)$

As mentioned in the Introduction, the electron-hole pairs are generated when TiO_2 is irradiated by UV photons with an energy higher than the TiO_2 band gap energy, and these charge carriers can then migrate to the TiO_2 surface to initiate various redox reactions of the adsorbates. Such interfacial electron (hole) transfer reactions are fundamental processes in various photocatalytic reactions.

Recently, it has been reported that $^1O_2(a^1\Delta_g)$ molecules are generated during the TiO_2 photocatalytic reactions [16–18]. As summarized in Scheme 2, the formation mechanisms of $^1O_2(a^1\Delta_g)$ can be described as the photocatalytic oxidation of superoxide ($O_2^{\bullet-}$) back to $^1O_2(a^1\Delta_g)$ molecules as follows: reaction (1), the conduction band (CB) electron, e^-, and the valence band (VB) hole, h^+, are generated after UV irradiation of TiO_2, reaction (2), $O_2^{\bullet-}$ is produced by the reduction of $^3O_2\left(X^3\Sigma_g^-\right)$ molecules with e^-, and reaction (3), $O_2^{\bullet-}$ is oxidized back to $O_2(a^1\Delta_g)$ molecule by h^+, resulting in $^1O_2(a^1\Delta_g)$ on the TiO_2 surface.

$$TiO_2 + h\nu \rightarrow TiO_2(h^+ \cdots e^-), \quad (1)$$

$$^3O_2\left(X^3\Sigma_g^-\right) + TiO_2(e^-) \rightarrow O_2^{\bullet-}, \quad (2)$$

$$O_2^{\bullet-} + h^+ \rightarrow {}^1O_2\left(a^1\Delta_g\right)\left(\text{or } {}^3O_2\left(X^3\Sigma_g^-\right)\right), \quad (3)$$

Otherwise, $O_2(a^1\Delta_g)$ is also generated by the energy exchange between the excited TiO_2 and $^3O_2\left(X^3\Sigma_g^-\right)$ molecules [18].

$$TiO_2 + h\nu \rightarrow TiO_2^*, \quad (4)$$

$$TiO_2^* + {}^3O_2\left(X^3\Sigma_g^-\right) \rightarrow TiO_2 + {}^1O_2\left(a^1\Delta_g\right), \quad (5)$$

However, this is considered not to be dominant when compared to that of the photocatalytic oxidation of $O_2^{\bullet-}$. In the remote TiO_2 photocatalytic oxidation, $^1O_2(a^1\Delta_g)$ generated on the TiO_2 surface is considered to barely diffuse into the gas phase forming airborne $^1O_2(a^1\Delta_g)$.

The remote TiO_2 photocatalytic oxidation has been applied to various inorganic and organic substrates such as the saturated alkyl chain monolayer and polymer [35–37], suggesting that only $HO^\bullet$ is capable enough to oxidize such diverse materials. More recently, Nosaka et al. successfully detected $HO^\bullet$ diffused in the gas phase from the photocatalytic TiO_2 surfaces using the in situ laser-induced fluorescence technique [33].

According to the literatures, it is strongly believed that ROS, such as $HO^\bullet$ and H_2O_2, are generated during the TiO_2 photocatalytic reactions, and diffused into the gas phase. To answer whether that the $HO^\bullet$ is sole reactive species or not, Majima et al. recently proposed a new strategy to detect the airborne ROS diffused from the surface of TiO_2 nanoparticles at the single-molecule level [58, 59].

Figure 4 shows the schematic illustration of the experimental setup for the detection of ROS with a single-molecule fluorescence probe (Alexa 532). The TiO_2 aqueous sol was coated on a slide glass by spin coating and the resulting TiO_2 film was calcined to obtain an optically opaque TiO_2-coated glass plate. The intervening gap was controlled using polyimide films. The TiO_2 coating was irradiated with a 100 W Hg lamp that passed through a band-pass filter (330–385 nm), an objective lens, and an Alexa 532 dye-modified coverslip.

Figure 5a shows the fluorescence images observed during the 532-nm excitation of single Alexa 532 dyes

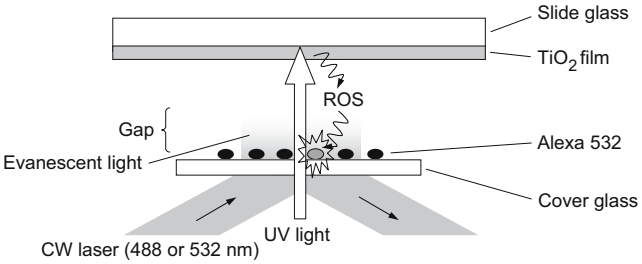

Fig. 4 Schematic illustration of the experimental setup for the detection of airborne ROS generated during TiO_2 photocatalytic reactions

before and after the UV irradiation of the TiO_2 film with the intervening gap of 12.5 μm in ambient air. The number of single fluorescence dyes (*N*) clearly decreased with the increasing UV irradiation time. It was found that the spatial distribution of ROS reaches about 100×100 μm^2 at the surface of the coverslip. In addition, as shown in Fig. 5b, the bleaching rates of the dyes significantly decreased with the increasing gap. It should also be noted that the bleaching of dyes was achieved by the very weak UV light. In the absence of a self-assembled monolayer of *N*-[3-trimethoxysilylpropyl]ethylenediamine (TSE) as a linker between the coverslip and the dye molecule, a significant decrease in the bleaching rate of dyes, which are spread over the cover glass using a spin coater, was observed. These results strongly support the fact that the degradation of dyes is caused by the bimolecular reaction with ROS, not by some artifacts such as the UV light scattering.

To identify the origin of ROS, they examined the influence of hole scavengers, such as 2-propanol, on the bleaching process of the dyes. The fluorescence images were obtained after UV irradiation of the TiO_2 film immersed in 2-propanol for 10 min. As shown in Fig. 5c, a significant decrease in the bleaching rate was clearly observed when compared with that obtained for bare TiO_2. The most likely explanation is that 2-propanol scavenges h^+ and/or $HO^\bullet$ generated at the surface of TiO_2 nanoparticles. Most importantly, it was found that a relatively low bleaching rate of single dye molecules immobilized onto a glass coverslip for the H_2O_2-coated glass was obtained, compared with the TiO_2-coated glass. These results clearly suggest that $HO^\bullet$ is *not* sole reactive species. Considering that gas diffusion coefficients of O_2 and $HO^\bullet$ in air are about 0.2 $cm^2\ s^{-1}$, the lifetimes of $HO^\bullet$ and $^1O_2(a^1\Delta_g)$, which are reported to be several tens or hundreds of milliseconds, seem to be sufficient to migrate at least up to the dye-modified coverslip [58].

To confirm the photocatalytic oxidation of single dyes with ROS, they observed single-molecule fluorescence spectra of dyes before and after the UV irradiation. As shown in Fig. 6a, it was found that the spectrum is blue shifted by approximately 15–20 nm after the UV irradiation. This blue shift also leads to the irreversible signal drop of the fluorescence signal. A similar spectral change was observed during the bleaching processes of dyes in a bulk aqueous solution, suggesting that the observed blue shift is due to the remote oxidation of single dyes by ROS. It should also be noted that the histogram of the peak wavenumber of the spectra observed after UV irradiation indicates two maxima around 17,820 and 18,380 cm^{-1}, which correspond to 561 and 544 nm, respectively (Fig. 6b). The former, which is almost identical with that (17,790 cm^{-1}, 562 nm) obtained before the UV irradiation, should be assigned to the unoxidized dyes. These experimental results strongly support multistep decomposition processes of dyes, i.e., further oxidation of the intermediate (oxidized) species, should be included in the remote photocatalytic oxidation processes of dyes.

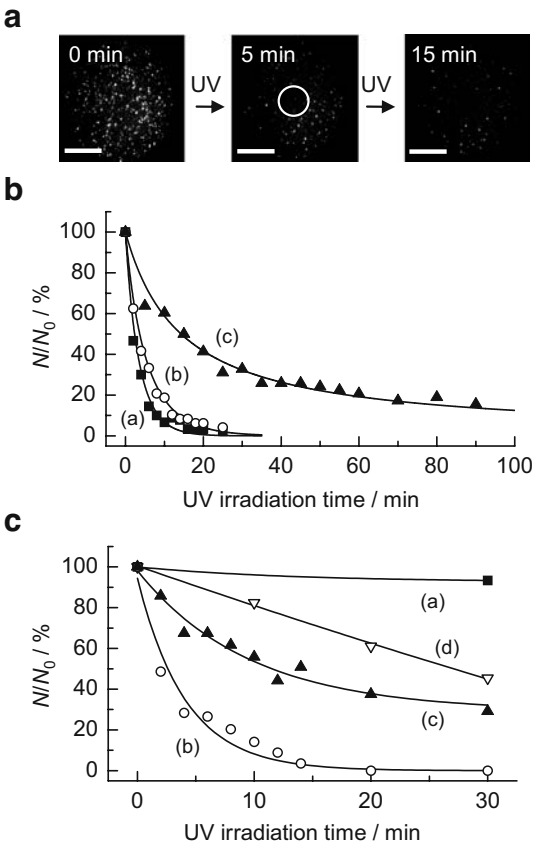

Fig. 5 **a** Fluorescence images observed during the 532-nm excitation of single dyes immobilized on the coverslip before and after UV irradiation (scale bars are 30 μm). The UV irradiation area is the inside of the white circle in the middle image. The bleaching of dyes at the center of the images is due to the UV irradiation. **b** Time dependence of the N/N_0 values in the gaps of 12.5 (*a*), 50 (*b*), and 125 (*c*) μm. The *solid lines* are visual guides. **c** Time dependences of the N/N_0 values in the 12.5 μm gap observed for the uncoated (*a*), the TiO_2-coated (*b*), the TiO_2-coated slide glasses immersed in 2-propanol (*c*), and the uncoated slide glass spin-coated with 30 wt % H_2O_2 (*d*). The *solid lines* are visual guides. Copyright 2005 American Chemical Society

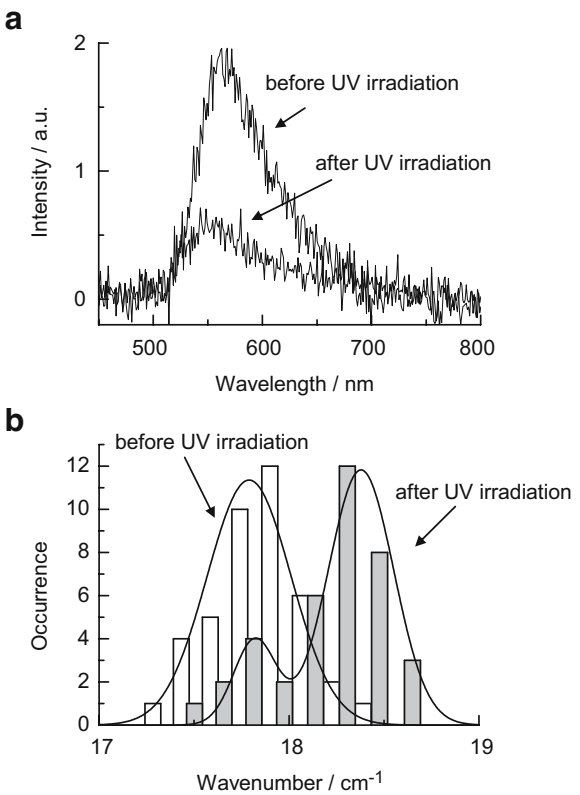

Fig. 6 **a** Typical single-molecule fluorescence spectra observed during the 488-nm excitation of the single dyes immobilized on the cover glass in the 12.5 μm gap before and after UV irradiation for 15 min. The spectra are cut below 510 nm by a long-pass filter on the blue edge. **b** Histogram of the peak wavenumber of the fluorescence spectra observed during the 488-nm excitation for the single dyes before and after UV irradiation for 15 min. *Solid lines* indicate Gaussian distributions fitted with the histograms. Copyright 2005 American Chemical Society

As a next step, Majima et al. successfully tried to detect an airborne $^1O_2(a^1\Delta_g)$ molecule diffused from the surface of TiO_2 nanoparticles using total internal reflection fluorescence microscopy (TIRFM) [59]. Although $^1O_2(a^1\Delta_g)$ molecules are believed to be generated during the TiO_2 photocatalytic reactions and the formation mechanism has been proposed as a mentioned above, there is no direct evidence to support the diffusion from the surface to the gas phase.

Their strategy to detect $^1O_2(a^1\Delta_g)$ molecules at the single-molecule level is summarized in Scheme 3 Terrylenediimide (TDI, the molecular structure is given in Scheme 3, although side chains, such as alkyl and phenyl groups, are substituted by hydrogen atoms for simplification) is used as the $^1O_2(a^1\Delta_g)$ sensor. According to the pioneer work, a single TDI molecule should be oxidized by a single $^1O_2(a^1\Delta_g)$ molecule to form a less fluorescent endoperoxide and successively a strongly fluorescent diepoxide with a spectral blue shift that is easily detected upon 532-nm laser excitation [46, 47].

Figure 7a depicted the single-molecule fluorescence images observed before and after UV irradiation of the TiO_2 film for 5 min. Before UV irradiation, only a few fluorescent spots were observed due to the weak fluorescence of the TDI excited at 532 nm. Due to the lack of sensitivity against the weak fluorescence, almost all TDIs cannot be recognized in the left image of Fig. 7a. Interestingly, after UV irradiation, bright fluorescent spots emerged around the UV-irradiated region as described by the white circles.

According to Scheme 3, these fluorescent spots would arise from the TDI diepoxide, which is formed by the cycloaddition reaction between the TDI and airborne $^1O_2(a^1\Delta_g)$ generated during the TiO_2 photocatalytic reactions. To clarify the formation of the TDI diepoxide, the single-molecule fluorescence spectra were measured for each spots before and after the UV irradiation as shown in Fig. 7b. Compared to that before UV irradiation, it was found that the spectrum after UV irradiation is blue-shifted by approximately 70 nm and has a strong fluorescence intensity. Thus, the bright fluorescent spots shown in the right image of Fig. 7a should be the TDI diepoxide, similar to a terrylene molecule reported by Basché et al [46]. The few bright spots in the left image of Fig. 7a also have a blue-shifted spectrum arising from the TDI diepoxide due to the self-sensitization. The fact that the TDI diepoxide shows a strong fluorescence intensity, when compared with that of TDI, is explained as the increase in the absorbed photon due to the blue shift of the absorption spectrum. There speculations were well supported by quantum calculations of optical transitions [59].

Figure 7c shows the histogram of the peak wavenumber of the fluorescence spectra before (upper panel) and after (lower panel) UV irradiation for 2 min. It should be noted that the histogram of the peak wavenumber of the spectra observed during UV irradiation indicates two maxima around 15,000 and 16,500 cm^{-1}, which are assigned to the parent TDI and TDI diepoxide, respectively. After UV irradiation, the number of TDI diepoxides, that is, the number of $^1O_2(a^1\Delta_g)$ molecules, clearly increased. It should also be noted that no further spectral blue shift due to multiple attacks of $^1O_2(a^1\Delta_g)$ was observed in the present wavelength range. Therefore, the bright spots in the fluorescence images can be regarded as a signal of single $^1O_2(a^1\Delta_g)$ molecules. This enables us to count the $^1O_2(a^1\Delta_g)$ molecules, although a part of $^1O_2(a^1\Delta_g)$ molecules might be deactivated in the PMMA film.

To clarify whether or not the digital switching occurs at the same position, the cross sections of the diffraction pattern before and after UV irradiation were obtained, as shown in Fig. 8. The TDI molecules that show the digital switching are indicated (see arrows in Fig. 8c). Some TDI molecules (for example, at 260 pixels) disappear after UV

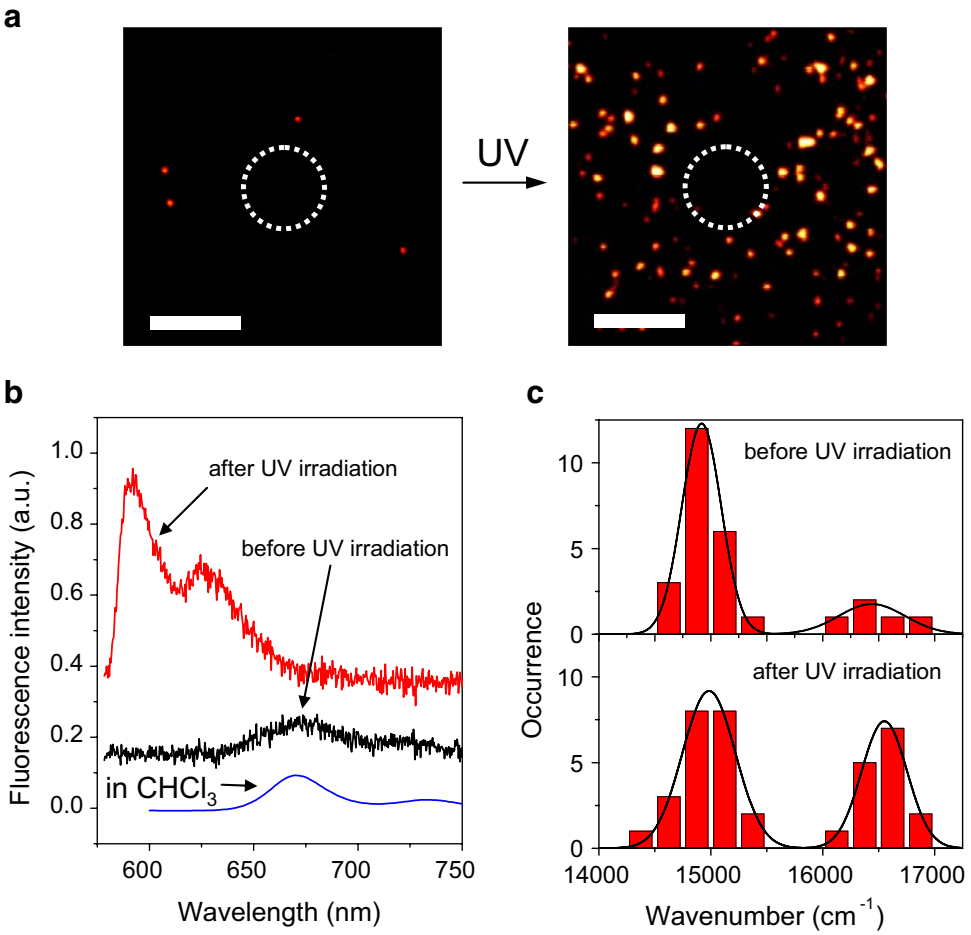

Fig. 7 **a** Fluorescence images of single TDIs spin-coated on the PMMA-coated coverslip before and after UV irradiation for 5 min (scale bars are 10 μm). The intervening gap is 12.5 μm. The *bright spots* correspond to the blue-shifted, TDI diepoxide. The UV irradiation area is inside the *white circle* in the images. The absence of dyes at the center of the image after UV irradiation is due to the bleaching of TDI caused by the direct UV irradiation. **b** Typical single-molecule fluorescence spectra of TDI before and after UV irradiation for 5 min. The intervening gap is 12.5 μm. The fluorescence spectra were obtained from excitation at 532 nm and cut below 580 nm by a long-pass filter on the blue edge. The fluorescence spectrum of TDI measured in $CHCl_3$ solution is shown for comparison. **c** Histogram of the peak wavenumber of the spectra observed before (*upper panel*) and after (*lower panel*) UV irradiation for 2 min. *Solid lines* indicate Gaussian distributions fitted with the histograms. Copyright 2006 American Chemical Society

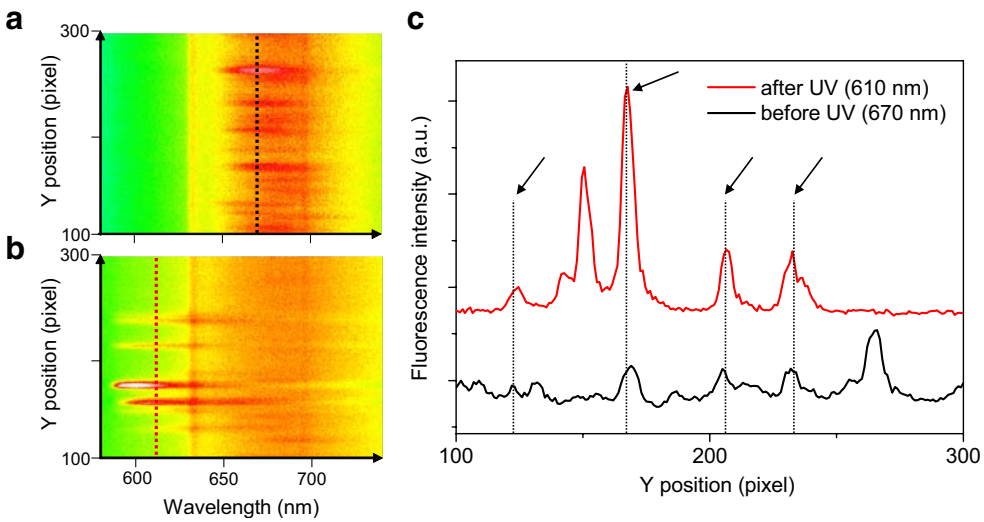

Fig. 8 The digital switching toward shorter wavelength arising from the oxidation of TDI during UV irradiation. The diffraction pattern of the single-molecule spectra before (**a**) and after (**b**) UV irradiation for 5 min. (**c**) The cross section of the diffraction pattern obtained before and after UV irradiation. The positions of the cross section before and after UV irradiation are indicated as *dotted lines* in **a** and **b**, respectively. The molecules that show the digital switching are indicated (see *arrows*). Copyright 2006 American Chemical Society

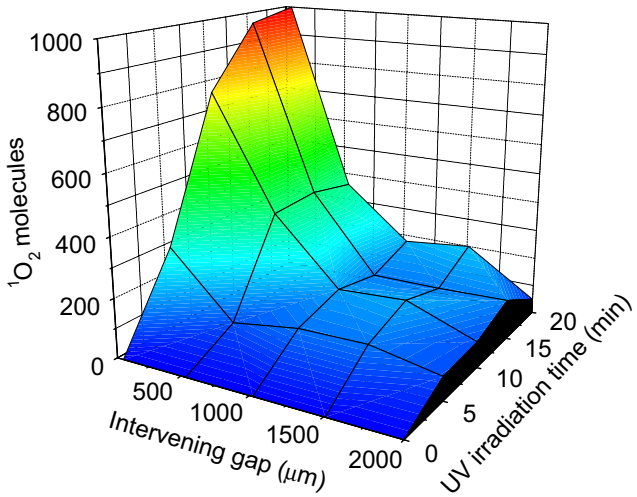

Fig. 9 The spatial and temporal distributions of $^1O_2(a^1\Delta_g)$ molecules diffused from the surface of TiO_2 film. The observation region is 70×70 μm^2. The intervening gaps are 50, 500, 1,000, 1,500, and 2,000 μm. Copyright 2006 American Chemical Society

irradiation. This would arise from the irreversible photobleaching. In contrast, after UV irradiation, two molecules (approximately 150 pixels) appear in which there is no molecule before the UV irradiation. This should be due to the addition of $^1O_2(a^1\Delta_g)$ to TDI, which is in the dark state, such as the triplet state, before UV irradiation. Under this experimental condition, 40% of the TDI molecules show complete digital switching.

Using this $^1O_2(a^1\Delta_g)$ nanosensor, the spatial and temporal distributions of single airborne $^1O_2(a^1\Delta_g)$ molecules diffused from the TiO2 film have been successfully investigated. Interestingly, several dozen $^1O_2(a^1\Delta_g)$ molecules are detected even at the intervening gap of 2,000 μm as shown in Fig. 9. To the best of our knowledge, this is the first example of the single-molecule detection of molecules traveling such a long distance in ambient air. The quantitative analysis enables us to estimate the generation efficiency of airborne $^1O_2(a^1\Delta_g)$ molecules during the TiO_2 photocatalytic reactions. They also calculated the $^1O_2(a^1\Delta_g)$ generation efficiencies during UV irradiation of 5, 10, 15, and 20 min of 11, 9.7, 8.4, and 6.5×10^{-9}, respectively, from the detected number of $^1O_2(a^1\Delta_g)$ and the number of photons absorbed by the TiO_2 film.

Single-molecule detection of H_2O_2

To date, the example for the detection of other ROS is really limited. In this section, we introduce a pioneering work on the detection of H_2O_2 at the single-molecule level.

Rigler et al. have studied single horseradish peroxidase (HRP) enzyme turnovers by fluorescence spectroscopy [60, 61]. Horseradish peroxidase (HRP) is an enzyme containing protoporphyrin IX as the key structural element. The iron ion incorporated in protoporphyrin IX participates in the redox cycle that initiates the decomposition of H_2O_2 and the reduction of donor molecules. They used dihydrorhodamine 6G as the hydrogen donor; this compound does not fluoresce itself but the product of its oxidation, rhodamine 6G, shows bright fluorescence. As shown in Fig. 10, to measure the avtivity of a single enzyme molecule, the HRP was immobilized on glass via a biotin-streptavidin interaction and placed into a buffer solution of calcium phosphate containing dihydrorhodamine 6G and H_2O_2 [60]. The fluorescence of the product was detected using a confocal type single-molecule fluorescence microscopy. According to experimental conditions, free rhodamine 6G molecules quickly departed from the laser-irradiated environment of the enzyme.

Figure 11 shows the typical traces of the substrate turnover of three single HRP molecules. The fluorescence bursts indicate the formation of rhodamine 6G molecules resulting from functioning of enzyme molecules. The fact that the product yield varies for each enzyme over the observation period of 10 s clearly indicates different activities of the three enzyme molecules. They explained that this fluctuation of the enzyme activity was attributed to different conformational states of the molecule. The conformational conversions of the enzyme change its activity and, hence, the product yield.

They also reported on single-molecule Raman and single-molecule fluorescence measurements of HRP using silver nanoparticles to enhance the optical signal, with an emphasis on biocompatibility of the nanoparticles [61].

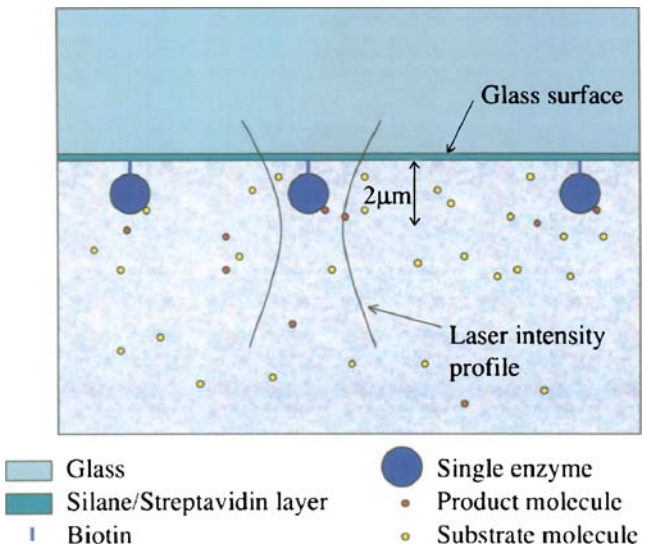

Fig. 10 Principal scheme for the measurements of single enzymes. The distance from the laser intensity maximum to the coverslip surface was adjusted to 2±0.5 μm for all measurements. Copyright 1999 Elsevier Science B.V.

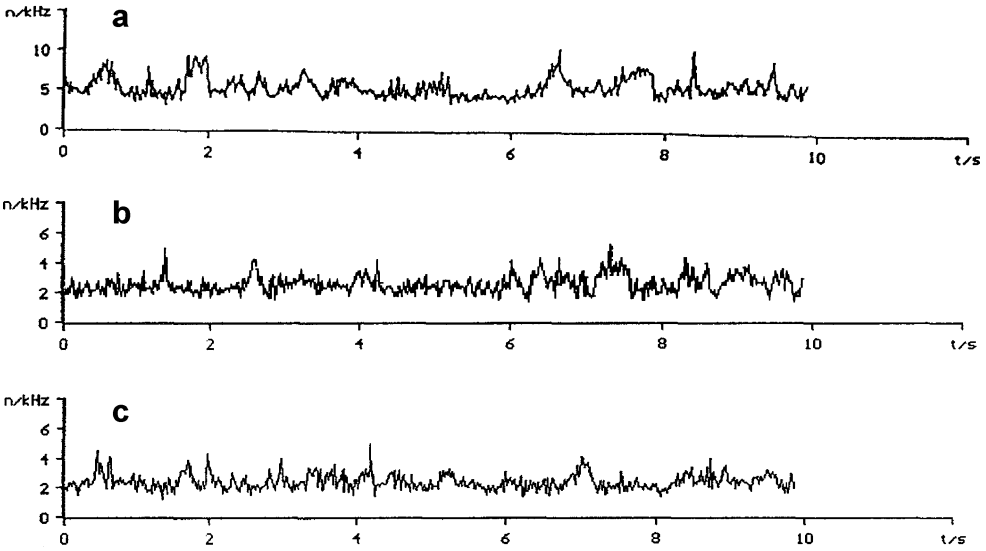

Fig. 11 Time traces for the photon number (n) emitted by rhodamine 6G synthesised by three single horseradish peroxidase molecules (**a**–**c**). The temporal change in product yield is attributable to the period of intensive functioning of the enzyme with resting periods. The enzyme molecules flicker in different ways, which is indicative of different activities of the three enzyme molecules. Copyright 1999 Elsevier Science B.V.

Future directions

Single-molecule fluorescence studies can reveal the detailed kinetics of physical processes and chemical reactions that are often hidden in ensemble measurements. We have successfully applied this technique to clarify the bleaching processes of single dye molecules during the remote TiO_2 photocatalytic reactions. Moreover, we detected an airborne $^1O_2(a^1\Delta_g)$ molecule diffused from the surface of the TiO_2 nanoparticles at the single-molecule level. This is a modern version of the Kautsky experiment using TiO_2 photocatalyst as a sensitizer [10].

In the future, the single-molecule spectroscopy will be applicable for various heterogeneous reaction systems as well as photocatalysts. The nanoscale inhomogeneities at the interface or on surface make it rather difficult for ensemble-averaged measurements to analyze the reaction dynamics. Recently, Hofkens and co-workers studied the spatial distribution of catalytic activity on a layered double hydroxide (LDH) consisting of prismatic crystals with large basal planes and lateral faces the entire crystal by using a wide field microscope (Fig. 12a) [62]. The obtained fluorescence intensity distribution clearly indicates that the hydrolysis activity follows the contours of the crystal (Fig. 12b). From experimental results, they concluded that ester hydrolysis proceeds on the lateral {1010} crystal faces, while transesterification occurs on the entire outer crystal surface. Such anisotropic behaviors would basically occur because of several factors; for example, a) the site or face-selective adsorption of agents, which is partially due to

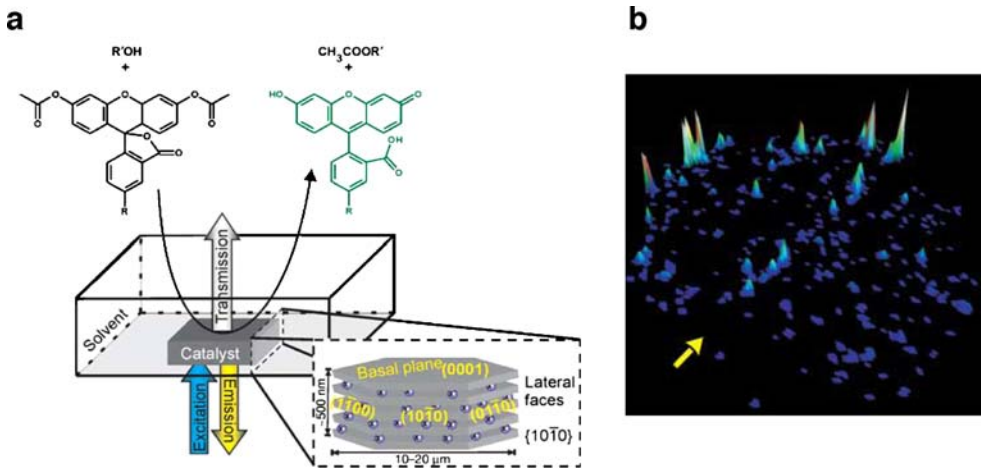

Fig. 12 **a** Schematic drawing of the experimental set-up: the LDH particle is exposed to fluorescein ester (R=−COOH for 5-carboxyfluorescein diacetate; R=−H for fluorescein diacetate) in R′OH solution (R'=−H for hydrolysis; R'=−nC_4H_9 for transesterification). A wide field microscope with 488 nm excitation light was used. The inset shows the different crystallographic faces of a hexagonal LDH crystallite with indication of the Miller indices. **b** Accumulated fluorescent spot intensity on the same crystal over 256 consecutive images. Copyright 2006 Nature Publishing Group

the heterogeneities of surface defect sites, and b) the site or face-specific catalytic reactivity, which is presumedly dependent on their electronic energy levels.

In addition, a range of powerful nanotechnologies, such as a lithographic technique, provide a novel method for observing and identifying individual molecules and particles [63]. The feasibility of studying heterogeneous reactions at the single-molecule level permits us to devise completely new experimental schemes. For instance, one can exploit the possibility to distinguish between the photocatalytically active and inactive molecules (particles). We believe that single-molecule (particle) experiments can provide novel information to understand heterogeneous photocatalytic reactions.

Conclusion

In this review, we have focused on the oxidation reactions of single dye molecules by ROS. The methodologies for the single-molecule detection of ROS, such as hydroxyl radical ($HO^{\bullet}$), singlet oxygen ($O_2(a^1\Delta_g)$), and hydrogen peroxide (H_2O_2), have been introduced together with examples. In particular, the methodology for the single-molecule detection of airborne $^1O_2$ molecules diffused from the surface of the TiO_2 nanoparticles was demonstrated. This single-molecule nanosensor will be applicable for the multiple detection of the ROS generated during various heterogeneous reactions, such as photocatalytic reactions.

Acknowledgments This work has been partly supported by a Grant-in-Aid for Scientific Research (Project 17105005, Priority Area (417), 21st Century COE Research, and others) from the Ministry of Education, Culture, Sports, Science and Technology (MEXT) of Japanese Government.

References

1. Pardini RS (1995) Toxicity of oxygen from naturally occurring redox-active pro-oxidants. Arch Insect Biochem Physiol 29: 101–118
2. Seinfeld JH, Pandis SN (1998) Atmospheric chemistry and physics. Wiley, New York
3. Wasserman HH, Murray RW (1979) Singlet oxygen. Academic, New York
4. Kearns DR (1971) Physical and chemical properties of singlet molecular oxygen. Chem Rev 71:395–427
5. Schweitzer C, Schmidt R (2003) Physical mechanisms of generation and deactivation of singlet oxygen. Chem Rev 103: 1685–1757
6. Adam W, Kazakov DV, Kazakov VP (2005) Singlet-oxygen chemiluminescence in peroxide reactions. Chem Rev 105: 3371–3387
7. Kautsky H, de Bruijn H (1931) The explanation of the inhibition of photoluminescence of fluorescent systems by oxygen: the formation of active, diffusing oxygen molecules by sensitization. Naturwissenschaften 19:1043
8. Kautsky H, Hirsch A (1931) Energy transformations on boundary surfaces, IV. Interaction of excited dyestuff molecules and oxygen. Chem Ber 64:2677–2683
9. Kautsky H, de Bruijn H, Neuwirth R, Baumeister W (1933) Energy transfers at surfaces, VII. Photosensitized oxidation as the action of an active, metastable state of the oxygen molecule. Chem Ber 66:1588–1600
10. Kautsky H (1939) Quenching of luminescence by oxygen. Trans Faraday Soc 35:216–219
11. Khan A, Kasha M (1963) Red chemiluminescence of oxygen in aqueous solution. J Chem Phys 39:2105–2106
12. Khan AU, Kasha M (1964) Rotational structure in the chemiluminescence spectrum of molecular oxygen in aqueous systems. Nature 204:241–243
13. Foote CS, Wexler S (1964) Olefin oxidations with excited singlet molecular oxygen. J Am Chem Soc 86:3879–3880
14. Corey EJ, Taylor WC (1964) A study of the peroxidation of organic compounds by externally generated singlet oxygen molecules. J Am Chem Soc 86:3881–3882
15. Kovalev D, Fujii M (2005) Silicon nanocrystals: photosensitizers for oxygen molecules. Adv Mater 17:2531–2544
16. Nosaka Y, Daimon T, Nosaka AY, Murakami Y (2004) Singlet oxygen formation in photocatalytic TiO_2 aqueous suspension. Phys Chem Chem Phys 6:2917–2918
17. Hirakawa K, Hirano T (2006) Singlet oxygen generation photocatalyzed by TiO_2 particles and its contribution to biomolecule damage. Chem Lett 35:832–833
18. Janczyk A, Krakowska E, Stochel G, Macyk W (2006) Singlet oxygen photogeneration at surface modified titanium dioxide. J Am Chem Soc 128:15574–15575
19. Samia ACS, Chen X, Burda C (2003) Semiconductor quantum dots for photodynamic therapy. J Am Chem Soc 125: 15736–15737
20. Bonnett R (1995) Photosensitizers of the porphyrin and phthalocyanine series for photodynamic therapy. Chem Soc Rev 24: 19–33
21. Fujishima A, Rao TN, Tryk DA (2000) Titanium dioxide photocatalysis. J Photochem Photobiol C: Photochem Rev 1:1–21
22. Paunesku T, Rajh T, Wiederrecht G, Maser J, Vogt S, Stojićević N, Protić M, Lai B, Oryhon J, Thurnauer M, Woloschak G (2003) Biology of TiO_2-oligonucleotide nanocomposites. Nature Mater 2:343–346
23. Clarke SJ, Hollmann CA, Zhang Z, Suffern D, Bradforth SE, Dimitrijevic NM, Minarik WG, Nadeau JL (2006) Photophysics of dopamine-modified quantum dots and effects on biological systems. Nature Mater 5:409–417
24. Fujishima A, Honda K (1972) Electrochemical photolysis of water at a semiconductor electrode. Nature 238:37–38
25. Ollis DF, Al-Ekabi H (eds) (1993) Photocatalytic purification and treatment of water and air. Elsevier, Amsterdam
26. Hagfeldt A, Grätzel M (1995) Light-induced redox reactions in nanocrystalline systems. Chem Rev 95:49–68
27. Hoffmann MR, Martin ST, Choi W, Bahnemann DW (1995) Environmental applications of semiconductor photocatalysis. Chem Rev 95:69–96
28. Linsebigler AL, Lu G, Yates Jr JT (1995) Photocatalysis on TiO_2 surfaces: principles, mechanisms, and selected results. Chem Rev 95:735–758
29. Thompson TL, Yates Jr JT (2006) Surface science studies of the photoactivation of TiO_2-new photochemical processes. Chem Rev 106:4428–4453
30. Ishibashi K, Nosaka Y, Hashimoto K, Fujishima A (1998) Time-dependent behavior of active oxygen species formed on photo-irradiated TiO_2 films in air. J Phys Chem B 102:2117–2120
31. Nosaka Y, Nakamura M, Hirakawa T (2002) Behavior of superoxide radicals formed on TiO_2 powder photocatalysts

studied by a chemiluminescent probe method. Phys Chem Chem Phys 4:1088–1092
32. Kubo W, Tatsuma T (2004) Detection of H_2O_2 released from TiO_2 photocatalyst to air. Anal Sci 20:591–593
33. Murakami Y, Kenji E, Nosaka AY, Nosaka Y (2006) Direct detection of OH radicals diffused to the gas phase from the UV-irradiated photocatalytic TiO_2 surfaces by means of laser-induced fluorescence spectroscopy. J Phys Chem B 110:16808–16811
34. Tatsuma T, Tachibana S, Miwa T, Tryk DA, Fujishima A (1999) Remote bleaching of methylene blue by UV-irradiated TiO_2 in the gas phase. J Phys Chem B 103:8033–8035
35. Tatsuma T, Tachibana S, Fujishima A (2001) Remote oxidation of organic compounds by UV-irradiated TiO_2 via the gas phase. J Phys Chem B 105:6987–6992
36. Kubo W, Tatsuma T, Fujishima A, Kobayashi H (2004) Mechanisms and resolution of photocatalytic lithography. J Phys Chem B 108:3005–3009
37. Kubo W, Tatsuma T (2006) Mechanisms of photocatalytic remote oxidation. J Am Chem Soc 128:16034–16035
38. Gomes A, Fernandes E, Lima JLFC (2005) Fluorescence probes used for detection of reactive oxygen species. J Biochem Biophys Methods 65:45–80
39. Ogilby PR (1999) Solvent effects on the radiative transitions of singlet oxygen. Acc Chem Res 32:512–519
40. Snyder JW, Zebger I, Gao Z, Poulsen L, Frederiksen PK, Skovsen E, McIlroy SP, Klinger M, Andersen LK, Ogilby PR (2004) Singlet oxygen microscope: from phase-separated polymers to single biological cells. Acc Chem Res 37:894–901
41. Snyder JW, Skovsen E, Lambert JDC, Poulsen L, Ogilby PR (2006) Optical detection of singlet oxygen from single cells. Phys Chem Chem Phys 8:4280–4293
42. Klembt Andersen L, Ogilby PR (2001) A nanosecond near-infrared step-scan Fourier transform absorption spectrometer: Monitoring singlet oxygen, organic molecule triplet states, and associated thermal effects upon pulsed-laser irradiation of a photosensitizer. Rev Sci Instrum 73:4313–4324
43. Zander C, Enderlein J, Keller RA (eds) (2002) Single molecule detection in solution: methods and applications. Wiley, New York
44. Xie XS, Trautman JK (1998) Optical studies of single molecules at room temperature. Annu Rev Phys Chem 49:441–480
45. Tinnefeld P, Sauer M (2005) Branching out of single-molecule fluorescence spectroscopy: challenges for chemistry and influence on biology. Angew Chem (Int Ed) 44:2642–2671
46. Christ T, Kulzer F, Bordat P, Basché T (2001) Watching the photo-oxidation of a single aromatic hydrocarbon molecule. Angew Chem (Int Ed) 40:4192–4195
47. Cotlet M, Vosch T, Habuchi S, Weil T, Müllen K, Hofkens J, De Schryver F (2005) Probing intramolecular förster resonance energy transfer in a naphthaleneimide-peryleneimide-terrylenediimide-based dendrimer by ensemble and single-molecule fluorescence spectroscopy. J Am Chem Soc 127:9760–9768
48. English DS, Furube A, Barbara PF (2000) Single-molecule spectroscopy in oxygen-depleted polymer films. Chem Phys Lett 324:15–19
49. Hou Y, Higgins DA (2002) Single molecule studies of dynamics in polymer thin films and at surfaces: effect of ambient relative humidity. J Phys Chem B 106:10306–10315
50. Mei E, Tang J, Vanderkooi JM, Hochstrasser RM (2003) Motions of single molecules and proteins in trehalose glass. J Am Chem Soc 125:2730–2735
51. Mei E, Vinogradov S, Hochstrasser RM (2003) Direct observation of triplet state emission of single molecules: single molecule phosphorescence quenching of metalloporphyrin and organometallic complexes by molecular oxygen and their quenching rate distributions. J Am Chem Soc 125:13198–13204
52. Lill Y, Hecht B (2004) Single dye molecules in an oxygen-depleted environment as photostable organic triggered single-photon sources. Appl Phys Lett 84:1665–1667
53. Zondervan R, Kulzer F, Kol'chenko MA, Orrit M (2004) Photobleaching of rhodamine 6G in poly(vinyl alcohol) at the ensemble and single-molecule levels. J Phys Chem A 108:1657–1665
54. Haase M, Hu1bner CG, Reuther E, Herrmann A, Müllen K, Basché Th (2004) Exponential and power-law kinetics in single-molecule fluorescence intermittency. J Phys Chem B 108: 10445–10450
55. Park SJ, Gesquiere AJ, Yu J, Barbara PF (2004) Charge injection and photooxidation of single conjugated polymer molecules. J Am Chem Soc 126:4116–4117
56. van Dijk MA, Kapitein LC, van Mameren J, Schmidt CF, Peterman EJG (2004) Combining optical trapping and single-molecule fluorescence spectroscopy: enhanced photobleaching of fluorophores. J Phys Chem B 108:6479–6484
57. Renn A, Seelig J, Sandoghdar V (2006) Oxygen-dependent photochemistry of fluorescent dyes studied at the single molecule level. Mol Phys 104:409–414
58. Naito K, Tachikawa T, Fujitsuka M, Majima T (2005) Single-molecule fluorescence imaging of the remote TiO_2 photocatalytic oxidation. J Phys Chem B 109:23138–23140
59. Naito K, Tachikawa T, Cui S-C, Sugimoto A, Fujitsuka M, Majima T (2006) Single-molecule detection of airborne singlet oxygen. J Am Chem Soc 128:16430–16431
60. Edman L, Földes-Papp Z, Wennmalm S, Rigler R (1999) The fluctuating enzyme: a single molecule approach. Chem Phys 247: 11–22
61. Bjerneld EJ, Földes-Papp Z, Käll M, Rigler R (2002) Single-molecule surface-enhanced raman and fluorescence correlation spectroscopy of horseradish peroxidase. J Phys Chem B 106: 1213–1218
62. Roeffaers MBJ, Sels BF, Uji-i H, De Schryver FC, Jacobs PA, De Vos DE, Hofkens J (2006) Spatially resolved observation of crystal-face-dependent catalysis by single turnover counting. Nature 439:572–575
63. Craighead H (2006) Future lab-on-a-chip technologies for interrogating individual molecules. Nature 442:387–393